CO2 Electrocatalyst Design Using Graph Theory

Ziyun Wang
Department of Electrical and Computer Engineering, University of Toronto, 10 King's College Road, Toronto, ON, M5S 3G4, Canada. https://orcid.org/0000-0002-2817-8367

Yuguang Li
Department of Electrical and Computer Engineering, University of Toronto, 10 King's College Road, Toronto, ON, M5S 3G4, Canada.

Jacob Boes
Stanford University, Department of Chemical Engineering, Stanford, California 94305, USA

Ying Wang
Department of Electrical and Computer Engineering, University of Toronto, 10 King's College Road, Toronto, ON, M5S 3G4, Canada.

Edward Sargent (ted.sargent@utoronto.ca)
Department of Electrical and Computer Engineering, University of Toronto, 10 King's College Road, Toronto, ON, M5S 3G4, Canada. https://orcid.org/0000-0003-0396-6495

Article

Keywords: electrochemical reduction, productization, propionaldehyde, acetone and hydroxyacetone

DOI: https://doi.org/10.21203/rs.3.rs-66715/v1

Abstract

The electrochemical reduction of CO_2 (CO_2RR) to higher-order hydrocarbons or oxygenates using low-carbon electricity offers a promising path to generate renewable fuels and chemicals; however, the low selectivity of present-day CO_2RR catalysts toward more valuable C_3 products limits technoeconomically compelling avenues toward productization. Systematically enumerating possible intermediates and reactions to the set of possible {C_1, C_2, and C_3} CO_2RR products entails 3206 intermediates and 4506 reactions. Here we use graph theory to enumerate these possibilities comprehensively, treating intermediates as graph nodes and pathways as graph edges. C_3 products fall into two groups, group A (1-propanol, allyl alcohol, and propionaldehyde) and group B (acetone and hydroxyacetone); and we find that an early branch reaction, three steps after C_1-C_2 coupling, bifurcates these two groups of C_3 products. We develop a set of C_3 descriptors and screen catalysts for CO2RR to C_3 products: specifically, we screen bimetallic (doped Cu) catalysts for their combination of CO binding, C_1-C_1 coupling and C_1-C_2 coupling. Cu and also Au- and Ag-doped Cu fulfill the first two requirements; but the set of promising C_1-C_2 coupling catalysts (Ni-doped Pb and Al-doped Pb) needed to get to C_3 is nonoverlapping with that for CO binding and C_1-C_1 coupling. Our findings agree with the experimental picture that Cu, while among the most productive to propanol, has been limited in F.E. to the 10-20% range; and that, to date, no single catalyst has achieved exceptional C_3 productivity. We discuss tandem catalyst designs where a first catalyst promotes CO binding and C_1-C_1, and where these C_2 and C_1 intermediates can come together for coupling on a second distinct class of integrated catalysts.

Introduction

The electrochemical reduction of carbon dioxide (CO_2RR) converts CO_2 to fuels and chemical feedstocks using renewable electricity[1]. CO_2RR can in principle produce a vast array of possible hydrocarbons and oxygenates: the carbon, oxygen, and hydrogen atoms from carbon dioxide and water are building blocks that constitute an extensive combinatorial space. Experimentally, only a few products have been reported to have high selectivity: these are carbon monoxide[2], formic acid[3], methane[4], ethylene[5], and ethanol[6]. Designing catalysts that go beyond these products is an important task in CO_2RR.

Rational catalyst design requires an understanding of reaction pathways to the desired product, and also to the competing products. Jaramillo and co-workers observed 16 different products with numbers of carbon from one to three (C_1-C_3) in CO_2RR on metallic copper catalysts[7]; yet the routes to these diverse products – such as, among C_3 products, hydroxyacetone, acetone, allyl alcohol, propionaldehyde, and 1-propanol – have not been reported.

For C_2 products, different groups report distinct reaction mechanisms: for example, C_1-C_1 coupling mechanisms have been proposed that range from OC-CO[8,9] to OC-COH[10] to OC-CHO[11,12] to OC-CHOH[12] and H_2C-CH_2.[13] The key intermediate species branching ethylene and ethanol pathways are also under

debate: Graza *et al.*[11] proposed that this bifurcation occurs immediately after OC-CHO coupling forming OCCHO* ($5e^-$ transferred from CO_2) on Cu(100). Goddard and co-workers[9] have suggested that HCCOH* ($8e^-$ transferred) is the key surface species on Cu(100) before the bifurcation of ethylene and ethanol. Calle-Vallejo and Koper[14] have reported that the key intermediate is H_2CCHO ($9e^-$ transferred).

The lack of authoritative mechanisms to C_3 products and debate over C_2 routes limits the rational design of new CO_2RR catalysts toward desired products: only once reaction pathways are known does it become feasible to pursue strategies to decrease the energies of intermediates along the pathways toward the desired product while increasing the energies of the intermediates in the competing pathways. For example, the design of CO_2RR catalysts with high ethylene selectivity requires knowledge of the C_1-C_1 coupling steps and the branch reactions to other C_2 products. This can inform the engineering of active sites that favour C_1-C_1 coupling and that limit branching to other products.

The number of possible reaction steps and intermediates in the CO_2RR up to C_3 species is large (**Figure 1a)**: there are 20 elementary steps in the pathway to 1-propanol, including 18 hydrogenation steps and 2 coupling steps. There are many possible choices *for each step*: for example, in the simple case from CO to CH_4, there are ten different pathways shown in **Figure 1b**. A comprehensive analysis of CO_2RR must enumerate systematically the possible intermediates and pathways. Further, a quantitative approach will be required: rather than reject certain pathways as unlikely, we propose a quantitative analysis of the energetics of each possible pathway.

We turned to graph theory[15] to enumerate the possibilities systematically, density functional theory (DFT) to calculate reaction energies, and a steady-state solver to evaluate the most favorable pathways. In a reaction network (**Figure 1b**), species (reactant, intermediates, and products) are represented as nodes; and reactions (edges) convert one species into another. Here we investigate CO_2RR to products up to and including C_3 on both Cu(111) and Cu(100).

Results And Discussions

Graph theory framework

We began from CO species since the activation of CO_2 to CO has been systematically investigated before[16,17]. We first obtained the possible chemical formulas up to the maximum carbon, oxygen and hydrogen atoms subject to $C \leq 3$, $H \leq 8$ and $O \leq 3$ (**Figure 2a**) using Catkit[18]. For each formula, we enumerated the possible structures and removed structures using the rules: no O-O, C-O-C, O-C-O bonds. As one example, the formula C_2H_2O (**Figure 2a**) has five different structures with oxygen and hydrogen at different positions. With this approach, we obtained 458 species: the structures, formula, and the number of electrons transferred from CO are listed in **Supplementary Sheet 1**.

We then calculated the formation energies of these species on Cu(111) and Cu(100). We chose the most unsaturated atom as the binding atom, and calculated the adsorption of the unsaturated species on the possible sites, including atop, bridge, hcp hollow and fcc hollow on Cu(111) and atop, bridge, and four-fold hollow on Cu(100) (**Figure 2b**), using an adsorption vector algorithm[18]. Following optimisation using DFT, we checked the connectivity matrix of the intermediates to ensure that there occurred neither dissociation nor reconstruction, and the dissociated or reconstructed species are removed from the species list. The effects of potential, solvent, and ions on the species formation energies are important, and there are several methods in literature to consider these effects, such as the ab initio molecular dynamics with biased sampling method[9], the grand canonical quantum mechanics (GCQM) method[8,19], charged water model using global optimization method[20], and implicit solvent model[21]. To consider the effects of solvent on the adsorption energies, we used the polarizable continuum model (PCM)[21] in surface adsorption calculations (**Supplementary Sheet 2**). The energy comparisions between the PCM and GCQM on Cu(111) and Cu(100) are shown in **Figure S1.** The most common reaction types are hydrogenation, C-C coupling, and water formation, in that order (**Figure 2c**). We checked the species pairwise to enumerate the possible reactions. For example, if species X and XH had the same structures except for one extra hydrogen, we added the reaction $X^* + H^+ \text{ « } XH^*$ to the reaction list. Using this algorithm, we consider the possible hydrogenation, coupling, and dehydroxylation reactions in CO_2RR up to C_3 products. 1144 hydrogenation reactions, 755 coupling reactions, and 354 dehydroxylation reactions were obtained (**Supplementary Sheet 3)**. The reactions containing unstable species were removed, resulting in 1616 reactions on Cu(100) and 1523 reactions on Cu(111), respectively.

With the formation energies of the possible species and the comprehensive reaction list, we then obtain the reaction energies (**Figure 2d**). We used the reaction energies in one pathway to describe the favourability of this pathway (more details are found in the Supplymentary Information). The effect of applied potential is considered with the computational hydrogen electrode,[22] and pH value is taken into account via the concentration of the reactant (proton source) in the steady-state solver (**Figure 2d**).

In sum, the reaction pathway search framework (**Figure 2**) generates structures of the species, calculates the adsorption structures of the intermediates, obtains the reaction energies, and builds the reaction graph using Catkit[18] and an *ab initio* simulation program (VASP)[23-26].

Reaction graph of CO_2RR

Figure 3a shows the reaction graph for CO_2RR, including the possible intermediates and products up to three carbons and their corresponding elementary steps. The number of C_1 species is 13 (**Figure 3a**), 55 for C_2 species, 385 for C_3 species, and 5 species without carbon. The species react with protons, forming other species with the same number of carbon atoms (black edges for hydrogenation and green edges for dehydroxylation in **Figure 3a**), or couple with other species to produce species with a higher number of carbons (red edges in **Figure 3a**). Except for methane, the products in **Figure 3a** are linked with more than one edge, suggesting that each product can be produced via several possible routes.

Using the simple path algorithm[27], we obtained the number of possible pathways for several products **(Table S1)**: for example, there exist 10 distinct pathways from CO to methane as shown in **Figure 1b**. Ethylene has 4744 different pathways from CO that are at least one intermediate different, while for CO to 1-propanol the possible pathways are more than 27 million. These make it infeasible to enumerate pathways manually.

In graph theory, the degree of the nodes refers to the number of edges connected to the nodes. This corresponds to the number of possible reactions in which a given species is implicated. The average degree of all nodes is ~13.2, and the maximum degrees are CH_2O and CH_3O, with 84 edges connected, suggesting that these two species are the most important in the reaction network from the point of view of connectivity. The high-degree species are C_1 species, since these species participate in coupling to form C_2 and C_3 species.

Formation energies of intermediates

The energy distributions of the intermediates are shown as a function of the number of electrons transferred in **Figure 3b**. The formation energy is referenced to the free energies of CO_2, H_2O, and H_2, which are the three reactants of CO_2RR. Thus, the formation energy of each intermediate in **Figure 3b** indicates the reaction energies for the step from CO_2 and H^+/H_2O to this intermediate. The number of electrons transferred per carbon atom indicates the degree of hydrogenation. In general, the formation energies increase first, and then decrease with further increase in the number of electrons transferred per carbon atom. Thus, the reaction energies of the first few steps are endothermic at low applied potential, indicating that the rate-determining step of $CO_{(2)}$RR is in the first few steps. When a negative potential is applied, the formation energies of the intermediates shift by the number of electrons transferred × potential: thus the overall reaction energies of intermediates with an electron transferred become more favourable. These results agree with the high overpotential due to the endothermic steps in the initial stages of CO_2RR. Favouring the first few steps using active site engineering enables the design of CO_2RR catalysts with low overpotential.

Figure 3b also shows that the formation energies of intermediates on Cu(100) are more stable than those on Cu(111), indicating that Cu(100) has a greater driving force for CO_2 reduction and is thus the more likely active site for CO_2RR[28]. The most energetically favourable pathway is in **Figure 3b**: it is the pathway from one intermediate to the most stable intermediate with one more electron transferred reachable in the graph. However, if the energies of two intermediates are similar, it is difficult to determine the one most likely in energy space; instead, it is necessary to obtain the most representative pathway(s) in rate space.

The formation energy distribution for intermediates having with 0-3 carbons is provided in **Figure 3c**. The median and the range of C_2 intermediate formation energy is lower than in the case of C_1 intermediate, and this is true both on Cu(111) and Cu(100). This suggests that C_2 is energetically favoured and is the main product of CO_2RR. Regarding C_2 to C_3, the driving force is much lower on both Cu(111) and Cu(100)

(**Figure 3c**), suggesting that it will be hard to make C_3 as the main product of CO_2RR on pure Cu catalysts. Experiments also show that Cu-based catalysts achieve high C_2 productivities in CO_2RR[5], and lower C_3 productivities[7].

C_2 Reaction mechanisms

C_1-C_1 coupling is the key step for the selectivity of the C_2 products[29]. Many different C_1-C_1 coupling reaction mechanisms are proposed including OC-CO[8,9], OC-COH[10], OC-CHO[11,12], OC-CHOH[12], H_2C-CH_2[13]. However, no conclusion has been drawn regarding the dominant elementary step for C_1-C_1 coupling. In our reaction graph, we considered all 55 C_1-C_1 possible coupling reactions on both Cu(111) and Cu(100). With the steady-state solver, we obtained the rates for the elementary steps up to C_2 including the C_1-C_1 coupling steps at different applied potentials from 0 to -1.5 V vs. standard hydrogen electrode (SHE).

Despite the large number of possible coupling reactions, there are only a few dominant C_1-C_1 coupling reactions. **Figure 4a and 4b** show the main C_1-C_1 coupling reactions and their likelihood among the C_2 formation steps at neutral pH and applied potential from 0 to -1.5 V vs. SHE. The C_1-C_1 coupling mechanisms change with applied potentials and facets due to changes in surface coverage. On Cu(100), OC-CO is the only possible pathway at 0 V, in agreement with the reaction step proposed in prior literature[8,9]. With an increase of applied potential, the hydrogenation steps become more favourable: thus, CO* is likely to be further hydrogenated. Therefore, the coverage of HCO* increases and the rate of OC-HCO coupling rises. In the applied potential region higher than -0.5 V, OC-HCO is the main reaction mechanism, a finding that has been reported by Nørskov and Head-Gordon[11,12]. The H_2CO-H_2CO and COH-COH coupling steps are also possible at high applied potential; however, these applied potential regions correspond to the formation of methane and hydrogen[30]. On Cu(111), CO-HCO is the main coupling step at potentials ranging from 0 V to -0.75 V, while CO-COH is also possible with a low likelihood (Figure 4b). HCO-HCO coupling takes the place of CO-HCO at more negative applied potentials.

The findings reported above span coupling mechanism in prior reports; and they conclude that there is not a single unique coupling mechanism. Instead, different coupling steps dominate at different conditions and facets.

We then went on to evaluate the set of paths to C_2 products. We show in Figure 4c the reaction mechanisms on Cu(100) to ethanol and ethylene, two main C_2 products for Cu-based catalysts of particular interest experimentally.[6,31] These are shown at -0.5 V and neutral pH. The reaction starts from CO-HCO coupling, forming OCCHO*, the most likely coupling mechanism at this condition (**Figure 4a**). The next steps are the hydrogenation of OCCHO* to OHCCHO* and then HOCHCHO*. The hydroxyl group in HOCHCHO* is then removed, giving HCCHO* and water. The removal of the second hydroxyl group happens at the intermediate HCCHOH*, and after the dehydroxylation reaction, HCCH* proceeds to ethylene with two more hydrogenation steps. This reaction pathway explains 49% of the ethylene formed. As an alternative next step following the dehydroxylation step, HCCHOH* can be hydrogenated to

H_2CCHOH* (**Figure 4c**). There are two main hydrogenation steps of H_2CCHOH* to H_2CCH_2OH* and H_3CCHOH*, both leading to the formation of ethanol. Interestingly, we found that the H_2CCH_2OH* can also form ethylene, similar to the mechanism reported by Koper and co-worker[14]. Therefore, more than one branch reaction exists between ethylene and ethanol on Cu(100) at U=-0.5 V vs. SHE and pH=7, and the HCCHOH* and H_2CCH_2OH* are the two key intermediates for the selectivity of these two products. The reaction pathways to all eight C_2 products on both Cu(100) and Cu(111) are listed in **Table S3-S18**.

C_3 Reaction mechanisms

As shown in **Table S1**, there exist 27 million different pathways from CO to 1-propanol. More carbon atoms mean more isomers due to the possible arrangements of carbon, hydrogen, and oxygen. We sought to enumerate the possible reaction pathways to C_3 products and explore the highest-rate paths.

The formation of C_3 species starts with C_1-C_2 coupling[32-34]. There are 700 coupling reactions for C_1-C_2 coupling due to the large numbers of possible C_2 species. We considered the coupling steps along with their ensuing reaction pathways to C_3 products. **Figure 5a** shows the reaction mechanism to five products reported experimentally[7] – 1-propanol, allyl alcohol, propionaldehyde, acetone, and hydroxyacetone – at U=-0.5 V and neutral pH; the reaction mechanisms to all ten C_3 products are found in **Supplementary Information** (Cu(100) in **Table S19-S28** and Cu(111) in **Table S29-S38**). The most favourable C_1-C_2 coupling mechanism at -0.5 V and neutral pH is OC-OCCHO coupling on Cu(100) (**Figure 5a**). Three hydrogenation steps follow the formation of OCC(O)CHO* (IM3_1 in **Figure 5a**), giving OHCC(O)CHOH* (IM3_3). The main branching steps occurs here, resulting in two groups of products: the hydrogenation of the middle oxygen to OHCC(OH)CHOH* (IM3A_1) leads to the formation of propionaldehyde, allyl alcohol, and 1-propanol (group A); while hydrogenation to HOCHC(O)CHOH* (IM3B_1) produces hydroxyacetone and acetone (group B).

Regarding the group A products, the first hydroxyl group removed in the C_3 species is on the middle carbon (**Figure 5a**). OHCCCHOH (IM3A_2) is then reduced to $OHCCHCH_2OH$* (IM3A_4) before the removal of the second hydroxyl group (Figure 5), forming $OHCCHCH_2$* (IM3A_5). This is followed by two possibilities: hydrogenation of CH_2- to CH_3- forming propionaldehyde, and hydrogenation of ketone group to the hydroxyl group. The branch between allyl alcohol and 1-propanol occurs at $HOCHCHCH_2$* (IM3A_7); then the 1-propanol is formed with three hydrogenation steps. For group B products, the bifurcation of hydroxyacetone and acetone happens at $HOCH_2C(O)CH_2$* (IM3B_4) (**Figure 5a**).

Interestingly, previous experiments[7] have suggested that partial current densities of these five C_3 products in CO_2RR also fall into two groups at pH=6.8 (**Figure 5b**): 1-propanol has the highest current density, followed closely by allyl alcohol and then propionaldehyde. The current densities to these three products (group A) are generally one order of magnitude higher than to the other two products, acetone and hydroxyacetone (group B). Furthermore, the branch reactions of 1-propanol and other C_3 products occurs in the following orders in the reaction process: {acetone, hydroxyacetone}, propionaldehyde, and allyl

alcohol. The current density ordered from lowest to highest proceeds acetone ≈ hydroxyacetone << propionaldehyde < allyl alcohol < 1-propanol.

In sum, there are two main branch reactions in the C_3 pathways: one at the initial stage after C_1-C_2 coupling, OHCC(O)CHOH* (IM3_3), leading two groups of products; and the other one occurs at the very end of the reaction process, $OHCCHCH_2$* (IM3A_5) and $HOCHCHCH_2$* (IM3A_7), and these give different products.

We also obtained information on reaction pathways to other C_3 products, including ones that have not been detected experimentally. Obtaining such results offers inputs into catalyst design beyond traditional products already seen in CO_2RR. For example, 1,2-propylene glycol is used in the production of polymers and food processing, and it has not been reported as a direct product of CO_2RR. Our results (**Figure 5a**) indicate that the 1,2-propylene glycol branches from the group B pathway at $HOCHC(O)CH_2$* (IM3B_3). If the intermediate state on one catalyst, $HOCHC(O)CH_3$ (IM3C_1), is more stable than $HOCH_2C(O)CH_2$ (IM3B_4), the catalyst may produce 1,2-propylene glycol. For such a design, the branching reaction energy differences to 1,2-propylene glycol vs. the competing products should be used as indicators in computational screening: the more negative the branching reaction, the more selective the catalyst. Other C_3 products pathways can be found in the **Supplementary Information**: 1,3-propylene glycol (Cu(100) in **Table S20** and Cu(111) in **Table S30**), propane (**Table S24** and **S34**), 2-propanol (**Table S25** and **S35**), glycerol (**Table S27** and **S37**).

Catalyst design for C_3 products

The framework presented herein allows systematic screening of possible pathways; we acknowledge that the use of reaction energies along the pathway as a surrogate for the favourability of a pathway is an approximation, and we recognize that, in future works, the graph theoretic enumeration can beneficially be combined with (for example) a high-throughput transition state searching method, kinetic Monte Carlo, high-level quantum chemistry, or machine learning.

With that caveat, we evaluate the implications of Figure 6 – a plot that captures CO binding (a), C_1-C_1 coupling (b), and C_1-C_2 coupling (c).

Optimal CO binding is reached near -0.67 V[35]. Not surprisingly, Cu (both pure and doped) comes closest to fulfilling this condition (**Figure 6a**). Au and Al include some doping options such as Pd-doped Au, Pd-doped Al, Ir-doped Al, and Rh-doped Al that come within 0.2 eV of the optimum.

Favourable C_1-C_1 coupling is the next prerequisite along the ultimate pathway towards C_3 products. Here the most strongly negative reaction energy in **Figure 6b** is the most desirable. Cu doped with Ag and with Au is promising here, and Al is particularly favourable, as Cu-doped Ag and Pb-doped Ag.

To go the rest of the way to C_3 products, a favourable reaction energy of C_1-C_2 coupling is further required. Here again the most strongly negative reaction energy is desired. Ni-doped Pb performs exceptionally well. Pure Cu is a reasonable candidate but not strongly favourable. Ag doped with Al, Au, and Pb, shows promise, but the C_1-C_2 coupling energy is not sufficiently strong as to favour C_3 formation overwhelmingly compared to Ni-doped Pb and Al-doped Pb.

Overall these findings are consistent with the observation that, in prior reports, Cu to propanol has been among the most productive, but its Faradaic efficiency has been limited to the 10-20% range; and that, to date, no single-material nor single-material-doped catalyst has achieved exceptional C_3 productivity.

Intriguingly, the finding that doping one catalyst with a single dopant does not simultaneously enable optimal CO binding; *and* highly reactive C_1-C_1 coupling; *and* C_1-C_2 coupling; suggests that a new strategy is needed to achieve productive C_3 generation.

One promising solution is tandem catalysts that combine two or more catalysts: a first catalyst (such as Cu) is in charge of CO* intermediate formation and C_1-C_1 coupling; and a second catalyst is specifically designed for C_1-C_2 coupling (in **Figure 6**, a candidate is Ni-doped Pb, though doped Au variants also suggest promise).

The enticing possibility of designing such tandem catalysts would require careful analysis of a number of considerations. If the first catalyst was responsible for both CO adsorption and C_1-C_1 coupling, it would then need to bind the C_2 intermediate with proper adsorption energy so that this could diffuse onto the second catalyst decorating the first. The average distance of an island of C_1-C_2 coupling catalyst from a given point on the C_1-C_1 coupling catalyst would need to be less than the in-plane diffusion length of the C_2 intermediate species for the intermediate to reach the C1-C2 region with high probability. The C_2 intermediate would need to "hop" to the C_1-C_2 coupling catalyst efficiently, as would a comparable density of C_1 intermediates. A full analysis of this possibility would require using the micro-kinetic modeling or kinetic Monte Carlo that took account of the different sites and their spatial distribution.

Conclusions

We enumerated herein the intermediates in CO_2RR up to $C_3H_8O_3$ on both Cu(111) and Cu(100). The most favourable reaction pathways were studied as a function of pH and applied potential. We obtained the intermediates in CO_2RR up to C_3 with the optimized structures. This offers candidates for experiment studies related to intermediates, such as in-situ Raman and infrared spectroscopy. We enumerated possible reaction pathways to 20 products, and 1144 hydrogenation reactions, 755 coupling reactions, and 354 dehydroxylation reactions were found. We found that the C_1-C_1 coupling mechanisms vary at different applied potentials and facets, including OC-CO, OC-HCO, H_2CO-OCH_2, and HOC-COH on Cu(100), and OC-HCO, OC-COH, and HCO-HCO coupling on Cu(111). This accounts for the diversity of C_1-C_1 coupling mechanisms in literature. Furthermore, the results also show there are two bifurcation steps

between ethanol and ethylene on Cu(100), and the key intermediate states branching two pathways are HCCHOH and H_2CCH_2OH.

We report systematically, for the first time, the suite of reaction pathways available to C_3 products. We found there exists two groups of products bifurcate at the early stage after C_1-C_2 coupling, namely group A (propionaldehyde, allyl alcohol, 1-propanol) and group B (acetone and hydroxyacetone). Previous experimental results showed that products in the same groups have similar partial current densities, and the partial current densities in the case of group A are an order of magnitude higher than those of group B.

We also obtained the reaction pathways to products not previously reported. These results offer the possibility to tune selectivity toward new chemicals and to design catalysts beyond those whose products are already known. The framework can be extended to more complicated products with higher numbers of carbon in CO_2RR and beyond. Based on these understanding, we offered designs of catalysts toward C_3 products.

Computational methods

Density functional theory calculations. In this work, the density functional theory (DFT) calculations were carried out with a periodic slab model using the Vienna ab initio simulation program[23-26] (VASP) (https://www.vasp.at/). Detailed theoretical methods are found in the Supplementary Information.

Declarations

Data availability

The datasets generated and analysed during the current study are available from the corresponding author on reasonable request.

Acknowledgements

This work was financially supported by TOTAL American Services, the Connaught Fund, the Ontario Research Fund: Research Excellence Program, the Natural Sciences and Engineering Research Council (NSERC) of Canada, and the CIFAR Bio-Inspired Solar Energy program. All DFT computations were performed on the IBM BlueGene/Q supercomputer with support from the Southern Ontario Smart Computing Innovation Platform (SOSCIP). SOSCIP is funded by the Federal Economic Development Agency of Southern Ontario, the Province of Ontario, IBM Canada, Ontario Centres of Excellence, Mitacs and 15 Ontario academic member institutions.

Author contributions

E.H.S supervised the project. Z.W. designed and carried out the DFT calculations. All authors discussed, commented on and revised the manuscript.

Competing financial interests: The authors declare no competing financial interests.

References

1 Hori, Y. Electrochemical CO_2 Reduction on Metal Electrodes. *Modern Aspects of Electrochemistry*, 89-189 (2008).

2 Liu, M. *et al.* Enhanced electrocatalytic CO_2 reduction via field-induced reagent concentration. *Nature***537**, 382-386 (2016).

3 Zheng, X. *et al.* Theory-guided Sn/Cu alloying for efficient CO_2 electroreduction at low overpotentials. *Nat. Catal.***2**, 55-61 (2019).

4 Manthiram, K., Beberwyck, B. J. & Alivisatos, A. P. Enhanced Electrochemical Methanation of Carbon Dioxide with a Dispersible Nanoscale Copper Catalyst. *Journal of the American Chemical Society***136**, 13319-13325 (2014).

5 Dinh, C.-T. *et al.* CO_2 electroreduction to ethylene via hydroxide-mediated copper catalysis at an abrupt interface. *Science***360**, 783-787 (2018).

6 Li, Y. C. *et al.* Binding site diversity promotes CO_2 electroreduction to ethanol. *Journal of the American Chemical Society***141**, 8584-8591 (2019).

7 Kuhl, K. P., Cave, E. R., Abram, D. N. & Jaramillo, T. F. New insights into the electrochemical reduction of carbon dioxide on metallic copper surfaces. *Energ. Environ. Sci.***5**, 7050-7059 (2012).

8 Goodpaster, J. D., Bell, A. T. & Head-Gordon, M. Identification of Possible Pathways for C–C Bond Formation during Electrochemical Reduction of CO_2: New Theoretical Insights from an Improved Electrochemical Model. *J. Phys. Chem. Lett.***7**, 1471-1477 (2016).

9 Cheng, T., Xiao, H. & Goddard, W. A. Full atomistic reaction mechanism with kinetics for CO reduction on Cu(100) from ab initio molecular dynamics free-energy calculations at 298 K. *Proc. Natl. Acad. Sci. U. S. A.***114**, 1795-1800 (2017).

10 Xiao, H., Cheng, T., Goddard, W. A. & Sundararaman, R. Mechanistic Explanation of the pH Dependence and Onset Potentials for Hydrocarbon Products from Electrochemical Reduction of CO on Cu (111). *Journal of the American Chemical Society***138**, 483-486 (2016).

11 Garza, A. J., Bell, A. T. & Head-Gordon, M. Mechanism of CO_2 Reduction at Copper Surfaces: Pathways to C_2 Products. *ACS Catal.***8**, 1490-1499 (2018).

12 Liu, X. *et al.* pH effects on the electrochemical reduction of CO_2 towards C_2 products on stepped copper. *Nat. Commun.***10**, 32 (2019).

13 Nie, X., Esopi Monica, R., Janik Michael, J. & Asthagiri, A. Selectivity of CO_2 Reduction on Copper Electrodes: The Role of the Kinetics of Elementary Steps. *Angew. Chem. Int. Ed.***52**, 2459-2462 (2013).

14 Calle-Vallejo, F. & Koper, M. T. M. Theoretical Considerations on the Electroreduction of CO to C_2 Species on Cu(100) Electrodes. *Angew. Chem. Int. Ed.***52**, 7282-7285 (2013).

15 Margraf, J. T. & Reuter, K. Systematic Enumeration of Elementary Reaction Steps in Surface Catalysis. *ACS Omega***4**, 3370-3379 (2019).

16 Cheng, T., Xiao, H. & Goddard, W. A. Reaction Mechanisms for the Electrochemical Reduction of CO_2 to CO and Formate on the Cu(100) Surface at 298 K from Quantum Mechanics Free Energy Calculations with Explicit Water. *Journal of the American Chemical Society***138**, 13802-13805 (2016).

17 Chernyshova, I. V., Somasundaran, P. & Ponnurangam, S. On the origin of the elusive first intermediate of CO_2 electroreduction. *Proc. Natl. Acad. Sci. U. S. A.* (2018).

18 Boes, J. R., Mamun, O., Winther, K. & Bligaard, T. Graph Theory Approach to High-Throughput Surface Adsorption Structure Generation. *J. Phys. Chem. A***123**, 2281-2285 (2019).

19 Xiao, H., Cheng, T. & Goddard, W. A. Atomistic Mechanisms Underlying Selectivities in C_1 and C_2 Products from Electrochemical Reduction of CO on Cu(111). *Journal of the American Chemical Society***139**, 130-136 (2017).

20 Montoya, J. H., Shi, C., Chan, K. & Nørskov, J. K. Theoretical Insights into a CO Dimerization Mechanism in CO_2 Electroreduction. *J. Phys. Chem. Lett.***6**, 2032-2037 (2015).

21 Mathew, K., Sundararaman, R., Letchworth-Weaver, K., Arias, T. A. & Hennig, R. G. Implicit solvation model for density-functional study of nanocrystal surfaces and reaction pathways. *The Journal of Chemical Physics***140**, 084106 (2014).

22 Nørskov, J. K. *et al.* Origin of the Overpotential for Oxygen Reduction at a Fuel-Cell Cathode. *J. Phys. Chem. B***108**, 17886-17892 (2004).

23 Kresse, G. & Furthmüller, J. Efficient iterative schemes for ab initio total-energy calculations using a plane-wave basis set. *Phys. Rev. B***54**, 11169-11186 (1996).

24 Kresse, G. & Furthmuller, J. Efficiency of ab-initio total energy calculations for metals and semiconductors using a plane-wave basis set. *Comp. Mater. Sci.***6**, 15-50 (1996).

25 Kresse, G. & Hafner, J. Ab-Initio Molecular-Dynamics Simulation of the Liquid-Metal Amorphous-Semiconductor Transition in Germanium. *Phys. Rev. B***49**, 14251-14269 (1994).

26 Kresse, G. & Hafner, J. Ab initio molecular dynamics for liquid metals. *Phys. Rev. B***47**, 558-561 (1993).

27 Dijkstra, E. W. A note on two problems in connexion with graphs. *Numer. Math.***1**, 269-271 (1959).

28 Jiang, K. *et al.* Metal ion cycling of Cu foil for selective C–C coupling in electrochemical CO_2 reduction. *Nat. Catal.***1**, 111-119 (2018).

29 Morales-Guio, C. G. *et al.* Improved CO_2 reduction activity towards C_{2+} alcohols on a tandem gold on copper electrocatalyst. *Nat. Catal.***1**, 764-771 (2018).

30 Huang, Y., Handoko, A. D., Hirunsit, P. & Yeo, B. S. Electrochemical Reduction of CO_2 Using Copper Single-Crystal Surfaces: Effects of CO* Coverage on the Selective Formation of Ethylene. *ACS Catal.***7**, 1749-1756 (2017).

31 De Luna, P. *et al.* Catalyst electro-redeposition controls morphology and oxidation state for selective carbon dioxide reduction. *Nat. Catal.***1**, 103-110 (2018).

32 Pang, Y. *et al.* Efficient electrocatalytic conversion of carbon monoxide to propanol using fragmented copper. *Nat. Catal.***2**, 251-258 (2019).

33 Zhuang, T.-T. *et al.* Copper nanocavities confine intermediates for efficient electrosynthesis of C_3 alcohol fuels from carbon monoxide. *Nat. Catal.***1**, 946-951 (2018).

34 Li, J. *et al.* Copper adparticle enabled selective electrosynthesis of n-propanol. *Nat. Commun.***9**, 4614 (2018).

35 Liu, X. *et al.* Understanding trends in electrochemical carbon dioxide reduction rates. *Nat. Commun.***8**, 15438 (2017).

Figures

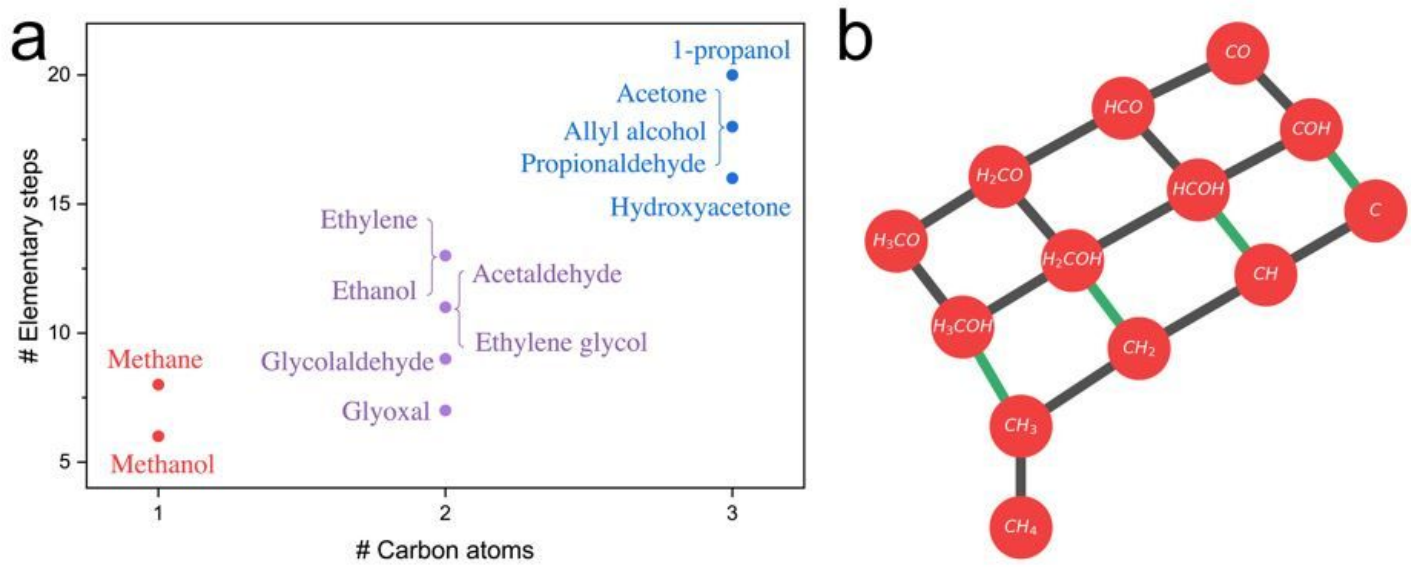

Figure 1

Complexity of reaction mechanisms. a. Relation between carbon atom number of CO2RR product and the elementary steps required to reach the product. b. Reaction network showing the reaction pathways from CO (top) to CH4 (bottom). Hydrogenation and deoxygenation reactions are shown in black and green, respectively.

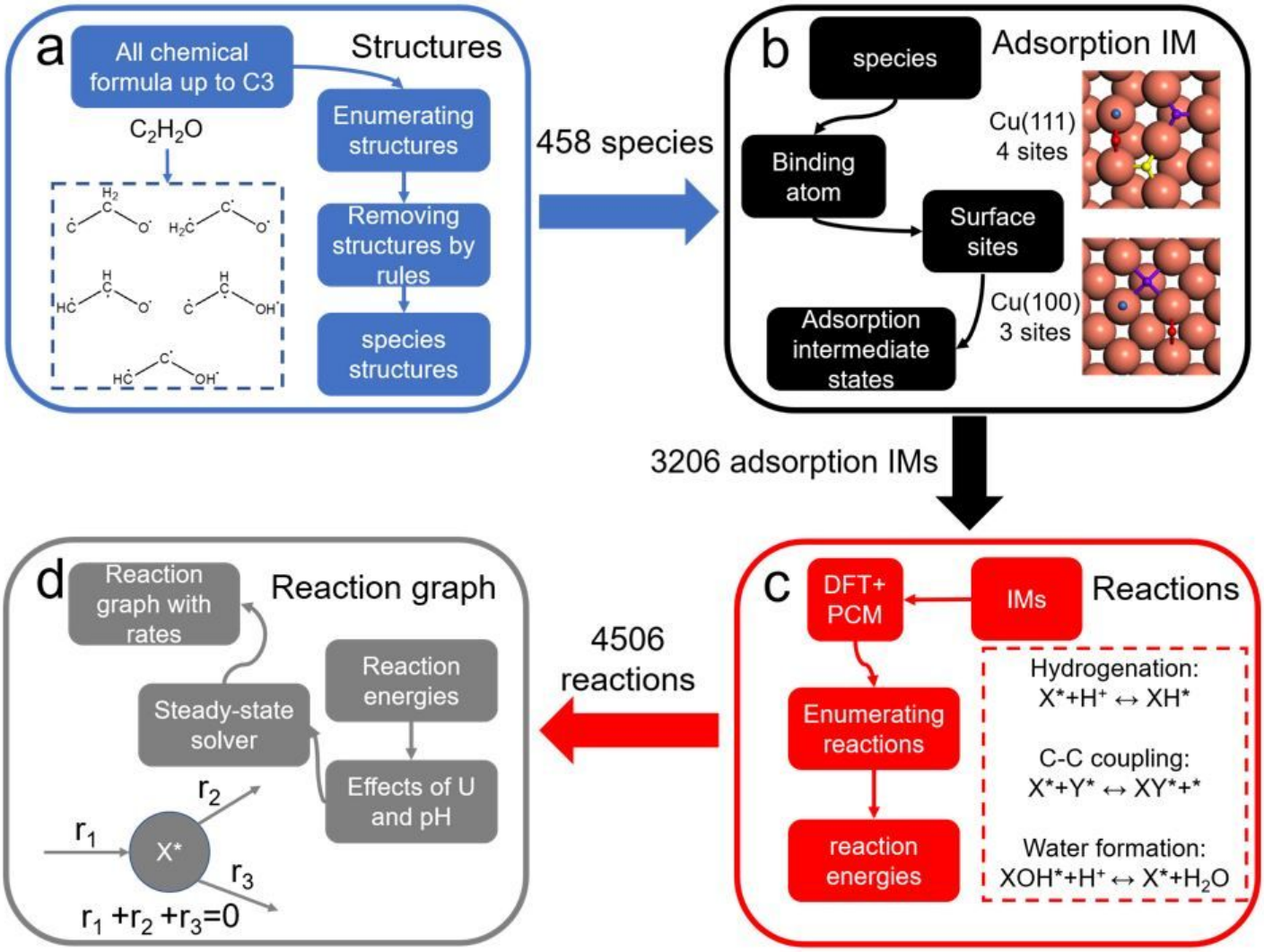

Figure 2

Computational pipeline. a. Enumeration of species structures. An example of different structures having the same chemical formula, C2H2O, is shown. b. Procedures to calculate the formation energies of intermediates on Cu(111) and Cu(100). c. Procedures to obtain the reactions and the corresponding reaction energies with DFT calculation and polarizable continuum model (PCM). d. Procedures to generate the reaction graph and obtain the reaction rates using a robust steady-state solver.

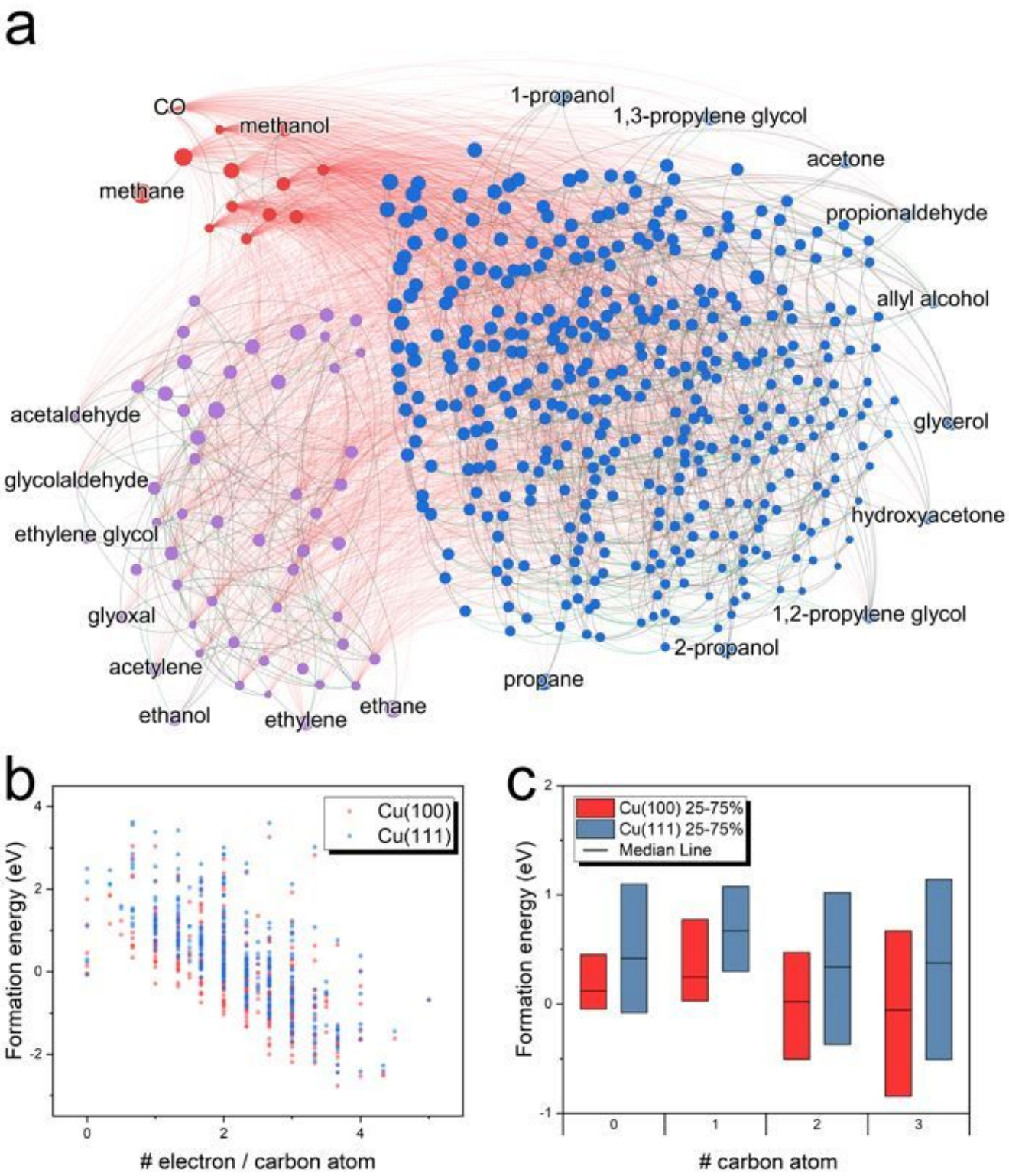

Figure 3

Reaction graph and formation energy distribution. a. Reaction graph from C1 to C3. Each node represents one reactant, intermediate or products; and each edge represents one reaction. Red, purple, and blue nodes stand for species with one, two, and three carbons, respectively. Coupling, hydrogenation, and dehydroxylation reactions are shown in red, black, and green, respectively. Formation energy distribution

of all the species on Cu(100) and C(111) according to b. the number of electron transfers per carbon atom and c. the number of carbon atoms.

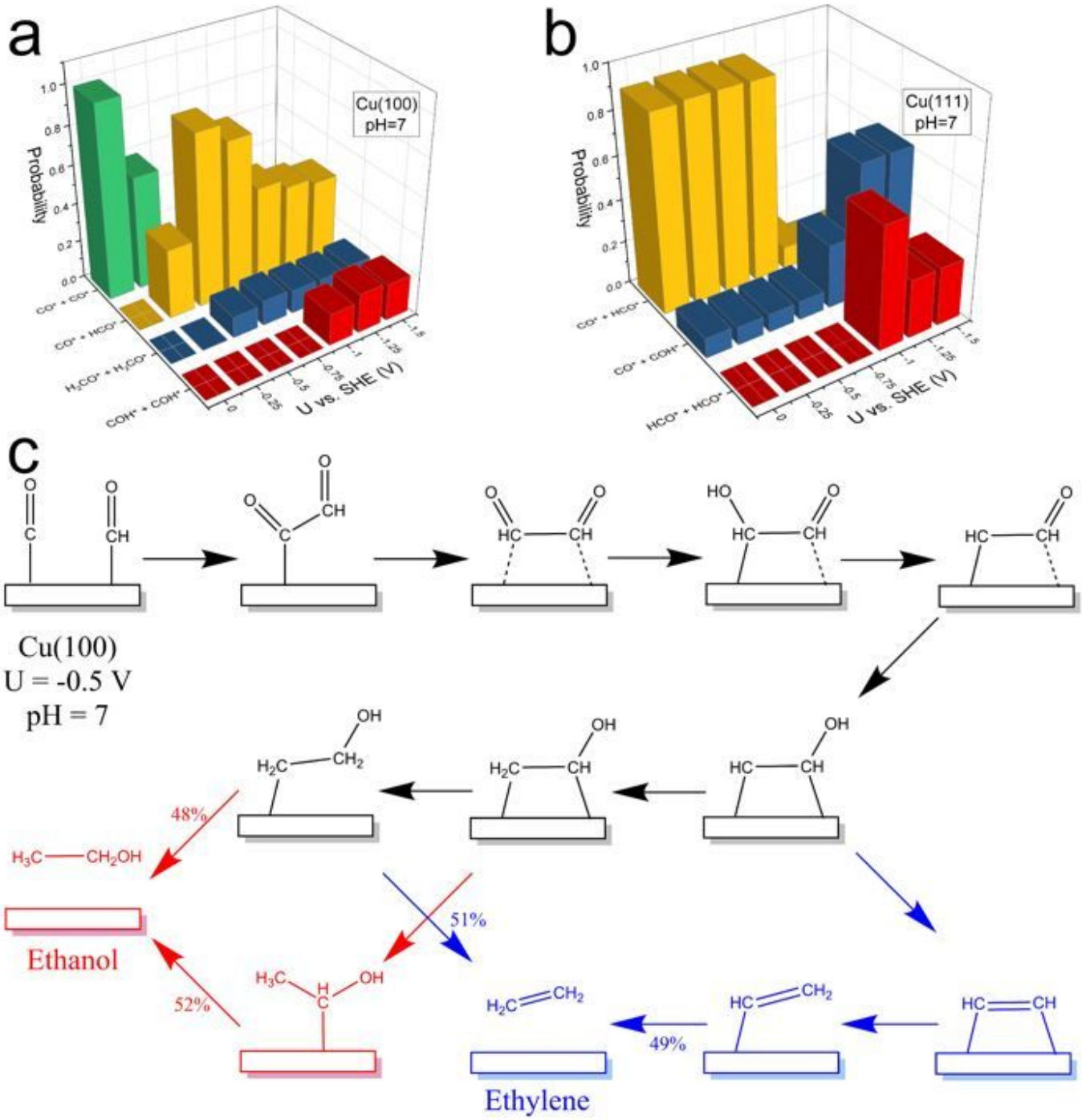

Figure 4

Reaction mechanisms of C2 formation. a-b. The set of possible C1-C1 coupling steps on (a) Cu(111) and (b) Cu(100) at pH = 7 and different applied potentials. c. The reaction mechanism of ethylene (blue) and ethanol (red) formation on Cu(100) at U = -0.5 V vs. SHE and pH = 7 obtained using graph theory.

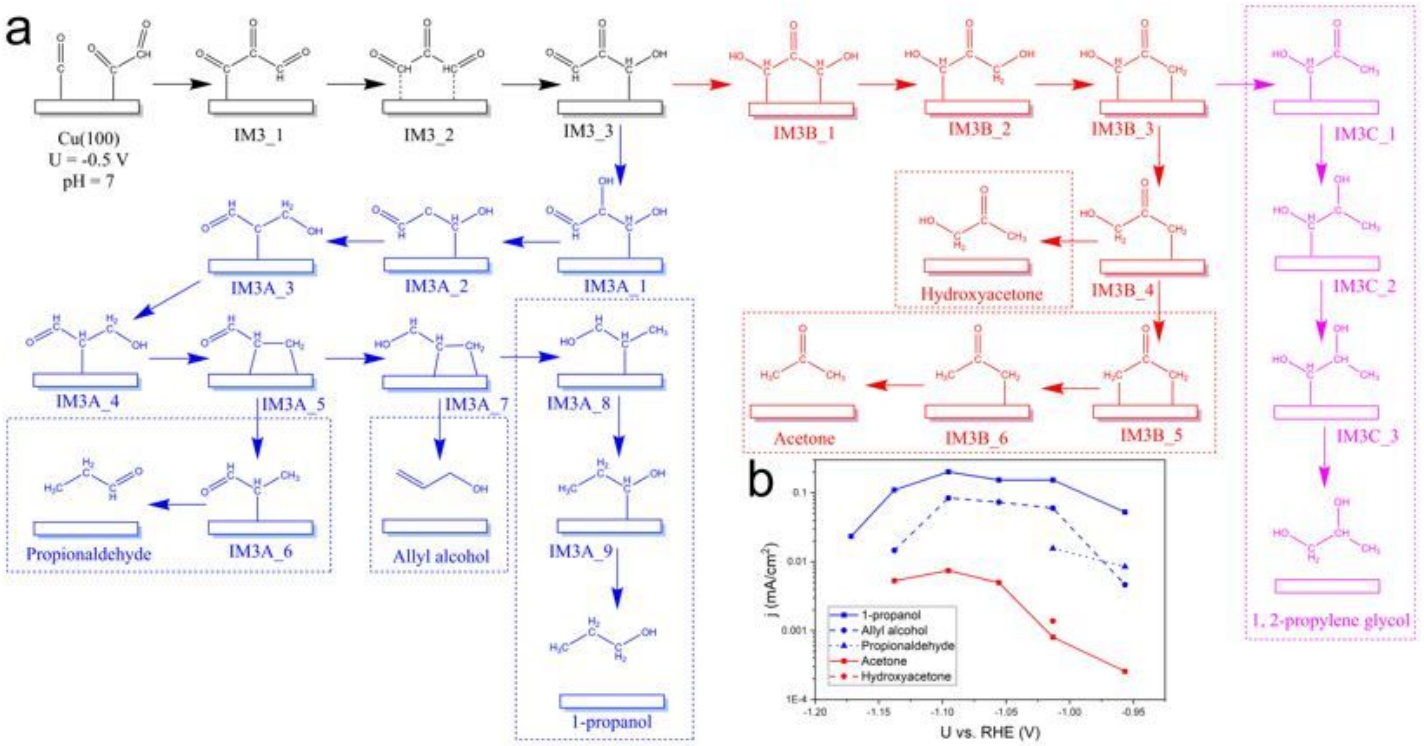

Figure 5

Reaction pathways of C3 products. a. The reaction mechanisms of two groups of C3 products, group A (blue, including 1-propanol, allyl alcohol, and propionaldehyde) and group B (red, including hydroxyacetone and acetone) on Cu(100) at U = -0.5 V vs. SHE and pH = 6.8, data are taken from ref. 7.

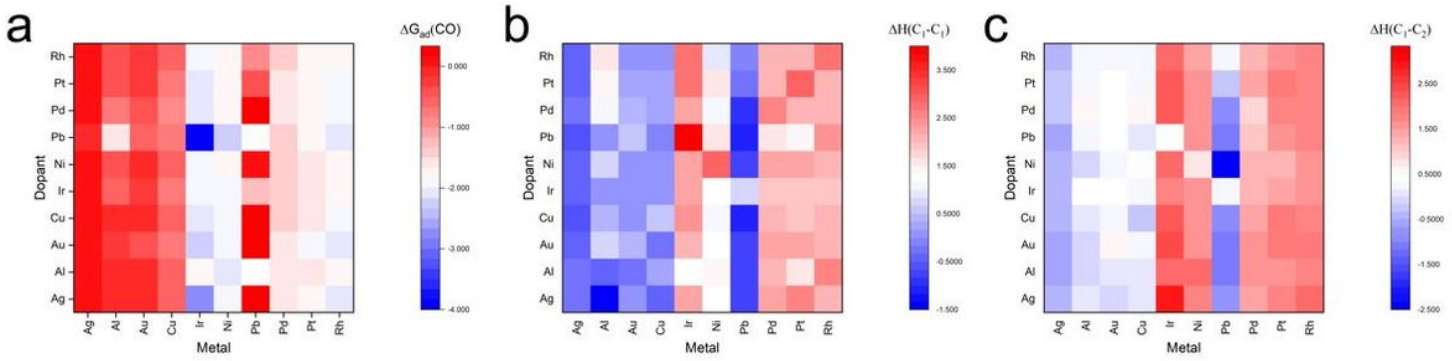

Figure 6

Screening of CO2RR catalysts of C3 products. a. The adsorption energy of CO, b. the reaction energy of C1-C1 coupling, c. the reaction energy of C1-C2 coupling on 100 screened alloy catalysts. All the energies are in eV.

Supplementary Files

This is a list of supplementary files associated with this preprint. Click to download.

- Supplementaryinformation.docx
- SupplementarySheet1Species.pdf
- SupplementarySheet2Energy.pdf
- SupplementarySheet3Reaction.pdf
- CuCO2RRDatabase.db